JOURNAL OF MATERIALS SCIENCE 16 (1981) 2717–2725

Gaseous reduction of an alloy oxide

JEFFREY S. ALLENDER
Savannah River Laboratory, E. I. duPont de Nemours Co. Inc., Aiken, South Carolina 29801, USA

LUTGARD C. De JONGHE
Materials and Molecular Research Division, Lawrence Berkeley Laboratory, and Department of Materials Science and Mineral Engineering, University of California, Berkeley, California 94720, USA

$Ni(Al, Fe)_2O_4$ ceramic alloys were reduced by hydrogen gas at a pressure of 1 atm, and at temperatures between 450 and 800° C. The reaction rate was determined from the rate of advance of the porous metal product layer–unreduced oxide interface. A simple analysis was presented permitting assessment of both the interface reaction resistance and the gas transport resistant through the porous product scales. The reaction was under mixed control in all conditions studied. In a range of temperatures and reaction times, preferred grain-boundary attack was observed. The conditions under which this was observed depended strongly on the Al^{3+} content of the ceramic alloy. Al^{3+} also lowered the interface reaction rate and inhibited scale coarsening by formation of dispersed unreduced phases in the product scales.

1. Introduction

When a dense oxide alloy reacts with a strongly reducing gas, such as hydrogen, a porous metal product layer can develop at its surface. If the gas flow is sufficient to eliminate the external mass transfer resistance, the pore structure of the metal layer and the nature of the metal–oxide interface reaction will determine the overall reaction-rate kinetics. When the reduction takes place directly from dense unreduced oxide to metal alloy, and the reaction is topochemical, a fairly simple reduction model may be applied [1, 2]. This model leads to layer growth kinetics described by

$$\dot{\xi} = \frac{p^0_{H_2}}{RTC_0}\left(\frac{\xi}{D_{eff}} + \frac{1}{k_r}\right)^{-1}, \qquad (1)$$

where ξ is the porous product layer thickness (cm), $\dot{\xi}$ is $d\xi/dt$ (cm sec^{-1}), $p^0_{H_2}$ is the hydrogen pressure in the gas stream (atm), R is the gas constant (atm cm^3 mol^{-1} K^{-1}), T is the temperature (K), C_0 is the oxygen concentration in the solid oxide (g-atom 0 cm^{-3}), D_{eff} is the effective gas diffusivity in the porous product layer (cm^2 sec^{-1}) and k_r is the interface reaction rate parameter (cm sec^{-1}). The details of the assumptions involved in this model have been discussed by Porter and De Jonghe [2]. The form of Equation 1 is similar to that developed first by Evans in 1924 [3] to describe the influence of the interface reaction on oxidation.

Comparison of the experimentally determined layer growth data with Equation 1 will thus permit a separation of the contributions to the overall reaction resistance of gas diffusion in the scale and of the interface reaction. This rate equation was recently used to study the details of the reduction reaction of cobalt ferrite [2]. The effects on the kinetics of substitutionally alloying the cobalt ferrite with aluminium were recently reported by Rey and De Jonghe [4]. It was found that in certain temperature ranges hard-to-reduce ions such as Al^{3+} promote extensive grain-boundary reduction and can inhibit pore coarsening in the product scale.

In this paper the reduction kinetics and product-phase morphologies of $NiFe_2O_4$ and $Ni(Al, Fe)_2O_4$ ceramic alloys are reported. Although Ni and Co are fairly similar elements, some interesting differences exist in the Ni–Fe–O and the Co–Fe–O

0022–2461/81/102717–09$02.90/0

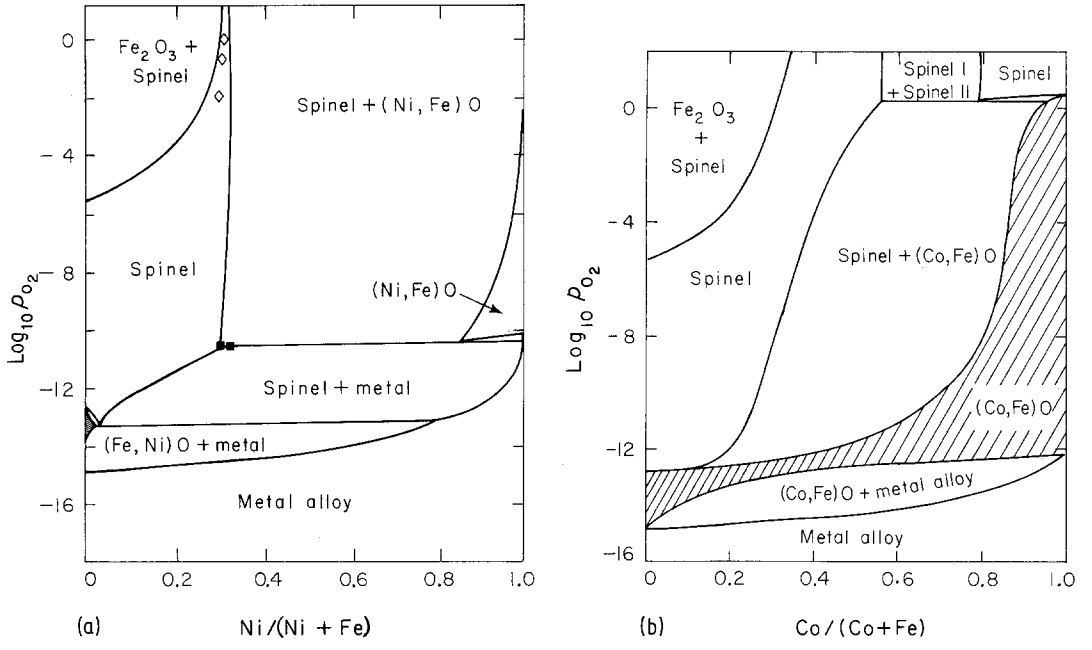

Figure 1 (a) Oxygen activity against composition diagram for nickel ferrites at 1000° C [7]. (b) Oxygen activity against composition diagram for cobalt ferrite [5]. The (Co, Fe)O and the (Ni, Fe)O fields have been shaded.

phase relationships that should affect the kinetics and micromorphology of the reduction. Comparison of the phase diagrams of nickel–iron oxides [5] and cobalt–iron oxides [6], in Fig. 1, shows that Ni is not significantly soluble in FeO, in contrast to Co, leading to different expected phases. In addition, Ni ions diffuse significantly more slowly than Co ions in their respective ferrite spinels at all oxygen activities [8].

2. Experimental procedure

The alloy oxides were dense polycrystalline $NiFe_2O_4$, $NiAl_{0.02}Fe_{1.98}O_4$, and $NiAl_{0.1}Fe_{1.9}O_4$. Grain sizes were between 4 and 8 μm. Porosities were about 2.5%.

Cube-shaped samples of edge length approximately 0.7 cm were placed in a platinum wire basket in a flow of hydrogen gas at 1 atm. The hydrogen gas contained less than 1 ppm of impurities. It was found that a flow rate of 2 cm sec^{-1} at the sample was sufficient to eliminate any dependence of reaction rate on mass transfer either to or from the sample surface at all reaction temperatures. After partial reduction, the samples were withdrawn from the hot zone of the furnace and were rapidly cooled in flowing hydrogen. This procedure effectively quenched the samples in their high-temperature morphology and prevented partial re-oxidation during cooling. Temperatures used in the reduction were 450, 500, 550, 600, 700, and 800° C.

After reaction, the partially-reduced specimens were cross-sectioned and polished, and the total product layer thickness was determined by optical microscopy. The specimens were briefly etched in a 2N HCl solution and re-examined. The etching solution selectively attacked the (Fe, Ni)O phase when present, but did not affect metal–alloy or spinel phases. Although some local variation in the interface position occurred, the movement of the average bulk–scale interface was sufficiently uniform to allow determination of a scale thickness with an error of less than 5%. The value reported for each scale thickness is an average of three to five replicate experiments; a total of about 500 reductions were carried out. The pore structures of the product scales were examined using a scanning electron microscope.

3. Experimental results and discussions

3.1. Kinetic measurements

The results of the layer measurements are shown in Figs 2 to 4. The product layer thicknesses after a reaction time of 3000 sec are compared in Fig. 5. For $NiFe_2O_4$ and $NiAl_{0.02}Fe_{1.98}O_4$, the increase of the interface advance rate diminishes in a temperature range between 500° C and 700° C. This decrease is, however, not comparable to the pro-

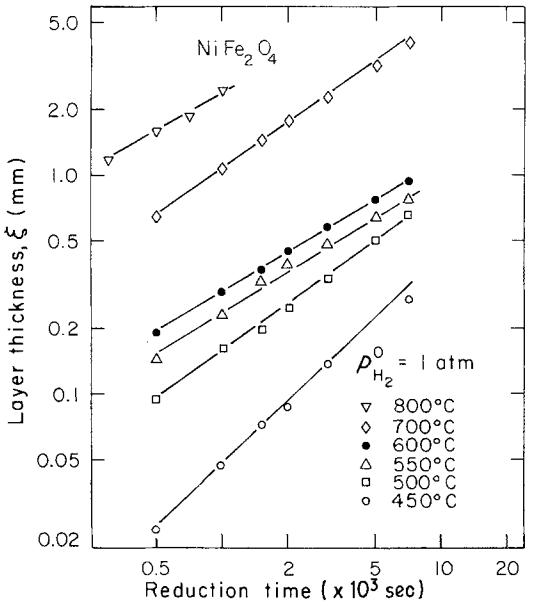

Figure 2 Total product layer thickness, ξ, as a function of time and temperature for hydrogen reduction of $NiFe_2O_4$. Each data point represents the average of 3 to 5 replicate experiments.

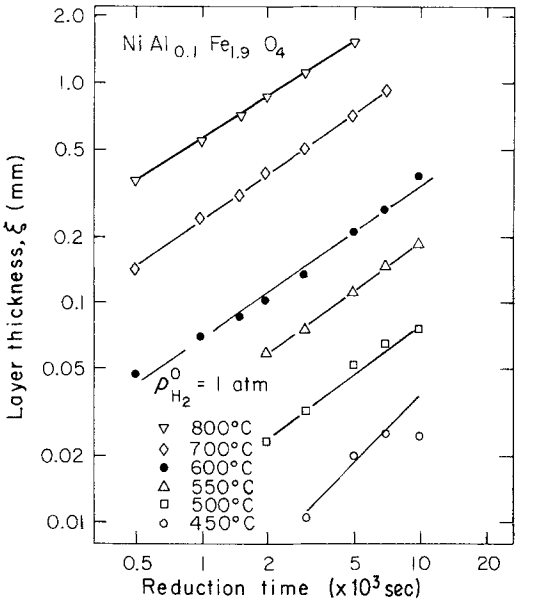

Figure 4 Total product layer thickness, ξ, as a function of time and temperature for hydrogen reduction of $NiAl_{0.1}Fe_{1.9}O_4$. Each data point represents the average of 3 to 5 replicate experiments.

nounced reaction rate minimum that was observed for cobalt ferrites in this temperature range. For $NiAl_{0.1}Fe_{1.9}O_4$ alloys, a reaction rate decrease is not observed. These results clearly demonstrate the pronounced effect of Al^{3+} on the reduction behaviour of the Ni–Al–Fe oxide alloys.

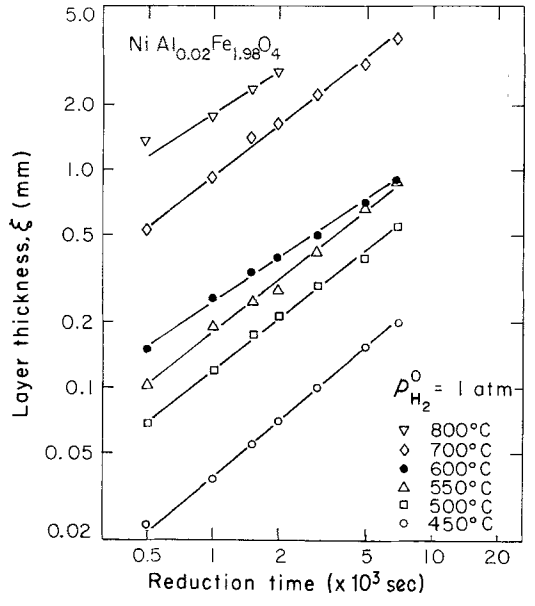

Figure 3 Total product layer thickness, ξ, as a function of time and temperature for hydrogen reduction of $NiAl_{0.02}Fe_{1.98}O_4$. Each data point represents the average of 3 to 5 replicate experiments.

To permit further analysis, Equation 1 can be integrated to give

$$a\xi^2 + b\xi = t, \tag{2}$$

where

$$a = \frac{C_0RT}{2D_{\mathrm{eff}}} \frac{1}{p^0_{H_2}} \tag{3}$$

and

$$b = \frac{C_0RT}{k_r} \frac{1}{p^0_{H_2}}. \tag{4}$$

The form of Equation 2 is similar to that used by Lu and Bitsianes [8].

Equation 2 can be further manipulated to give

$$b/a = (t_2\xi_1^2 - t_1\xi_2^2)/(t_1\xi_2 - t_2\xi_1), \tag{5}$$

where ξ_1 and ξ_2 are the values of ξ after times t_1 and t_2. From Equation 2 it also follows that

$$a = t/(\xi^2 + b\xi/a). \tag{6}$$

Thus, D_{eff} and k_r can be found from Equations 3 to 6. We also note that when

$$\xi = \xi_c \simeq b/2a \tag{7}$$

then

$$\xi_c \simeq D_{\mathrm{eff}}/k_r. \tag{8}$$

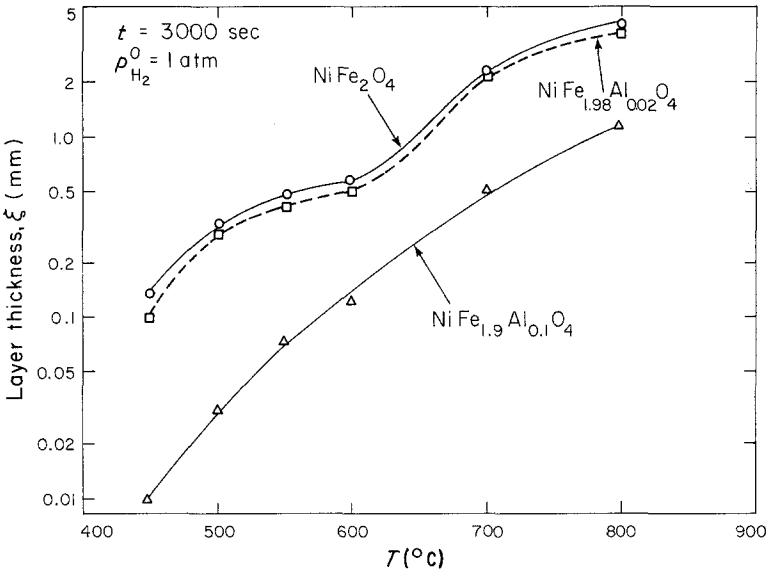

Figure 5 Total product layer thickness, ξ, measured after 3000 sec as a function of temperature, T (° C), for reduction with hydrogen.

At this product layer thickness, ξ_c, the gas diffusion resistance and the interface reaction resistance contribute equally to the control of the overall reduction kinetics. Thus, the reaction will be mainly under interface reaction control when $\xi \ll b/2a = \xi_c$, and will be under gas transport control when $\xi \gg \xi_c$.

Application of this analysis to the data obtained for the reduction of nickel ferrites yielded the results shown in Table I.

Comparison of these values of ξ_c, listed in Table I, with the data plotted in Figs 2 to 4 clearly indicates that the reactions are under mixed control in the temperature and time intervals of the measurements. In addition, for the measurement interval reported here, the importance of the gas transport resistance through the porous scale increases with increasing temperature.

Calculated values of D_{eff} are shown in Fig. 6. D_{eff} for $NiFe_2O_4$ and $NiAl_{0.02}Fe_{1.98}O_4$ does not vary simply with temperature. Below 500° C, D_{eff} decreases rapidly with decreasing temperature while, above 500° C, D_{eff} changes only little. Values of D_{eff} above 500° C could not be obtained for these materials since the microstructural examination of the scales, reported below, showed that the model underlying Equation 1 was no longer valid. The values for D_{eff} for $NiAl_{0.02}Fe_{1.98}O_4$ were generally lower than those for $NiFe_2O_4$. It is interesting to compare the effective gas diffusion coefficients for the transport through the porous product layer, D_{eff}, for $NiFe_2O_4$ and for $CoFe_2O_4$ [3] at 600° C: $D_{eff} \simeq 0.005$ for nickel ferrite, while $D_{eff} \simeq 0.4$ for cobalt ferrite. This difference implies significantly different pore structures for the product scales of these two materials.

In recent work by Chang and De Jonghe [9] in which the dependence of k_r on gas pressure and temperature was examined for gaseous reduction of $CoFe_2O_4$, it was shown that the interface reaction was a combination of a gas–solid surface reaction coupled with an interface solid-state transport step.

The values of k_r for nickel aluminium ferrites are shown in Fig. 7. k_r appears to follow a simple Arrhennius relationship, suggesting that the same interface process occurs for the temperature domain in which Equation 1 is valid. The apparent activation enthalpy for k_r for $NiFe_2O_4$ and for

TABLE I Product layer thickness, ξ_c, at which the gas diffusion and the interface reaction contribute equally to the total reaction resistance for different materials and temperatures

Material	ξ_c (mm)					
	450° C	500° C	550° C	600° C	700° C	800° C
$NiFe_2O_4$	0.4	0.45	0.19	0.13	–	–
$NiAl_{0.02}Fe_{1.98}O_4$	0.21	0.36	0.25	0.17	–	–
$NiAl_{0.1}Fe_{1.9}O_4$	–	0.06	0.07	0.04	0.13	0.24

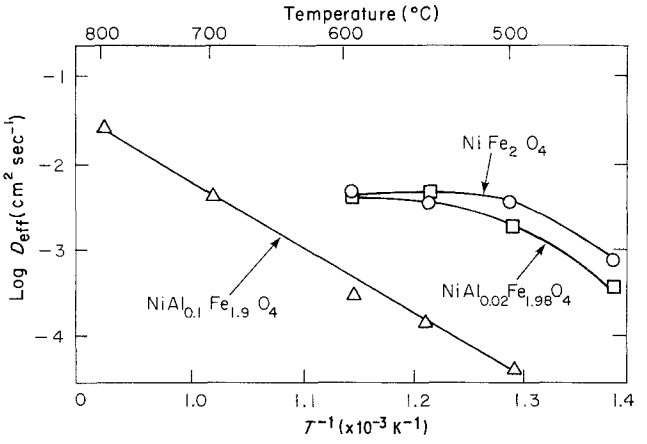

Figure 6 The effective gas diffusion coefficient, D_{eff}, for transport through the porous product layer. Above 600° C the values of D_{eff} for $NiFe_2O_4$ and $NiAl_{0.02}Fe_{1.98}O_4$ could not be calculated since the scales were no longer single-phase.

$NiAl_{0.02}Fe_{1.98}O_4$ is 10 kcal mol^{-1}, while for $NiAl_{0.1}Fe_{1.98}O_4$ it is 12 kcal mol^{-1}. The main action of Al^{3+} alloying additions thus appears to be the depression of the pre-exponential factor of the interface reaction-rate parameter. This may be due to the formation of small iron aluminate precipitates at the reaction interface, so that the number of active reaction sites accessible to the reducing gas is lowered. Formation of iron aluminate precipitates is to be expected since they were also formed in the gaseous reduction of cobalt ferrites alloyed with Al^{3+} [3]. A wider range of experiments should be performed on ceramic oxide alloys to fully clarify the role of the precipitates on interface reactions.

3.2. Micromorphology of the product layers

A range of microstructures was observed in the reaction product layers of the different alloy oxides. These microstructures are dependent upon temperature, composition, and reaction time. In general, at the lower reaction temperature all scales consisted simply of a porous metal alloy. At temperatures above 600° C, the scales that formed on $NiFe_2O_4$ and $NiAl_{0.02}Fe_{1.98}O_4$ were more complex and proved to be of a two-phase type.

3.2.1. $NiFe_2O_4$

Up to about 600° C the metal product layers formed on this material were single-phase and exhibited a clear reaction interface. At 600° C, i.e., above the (Fe, Ni)O stability temperature, a single-phase porous metal scale initially formed, with a clear spinel–metal interface. However, after long reaction periods the metal phase formed preferentially along the original spinel boundaries and unreduced oxide was partly retained. Etching

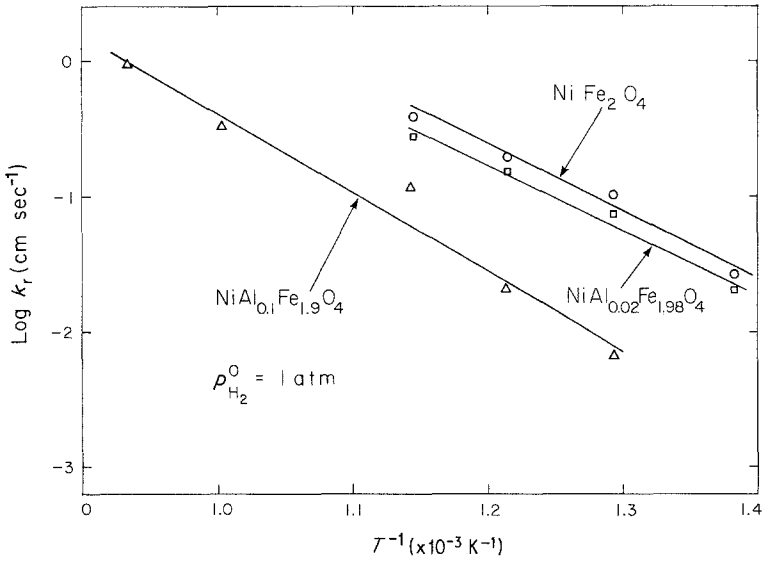

Figure 7 The interface reaction rate parameter, k_r, for nickel aluminium ferrite by hydrogen as a function of temperature.

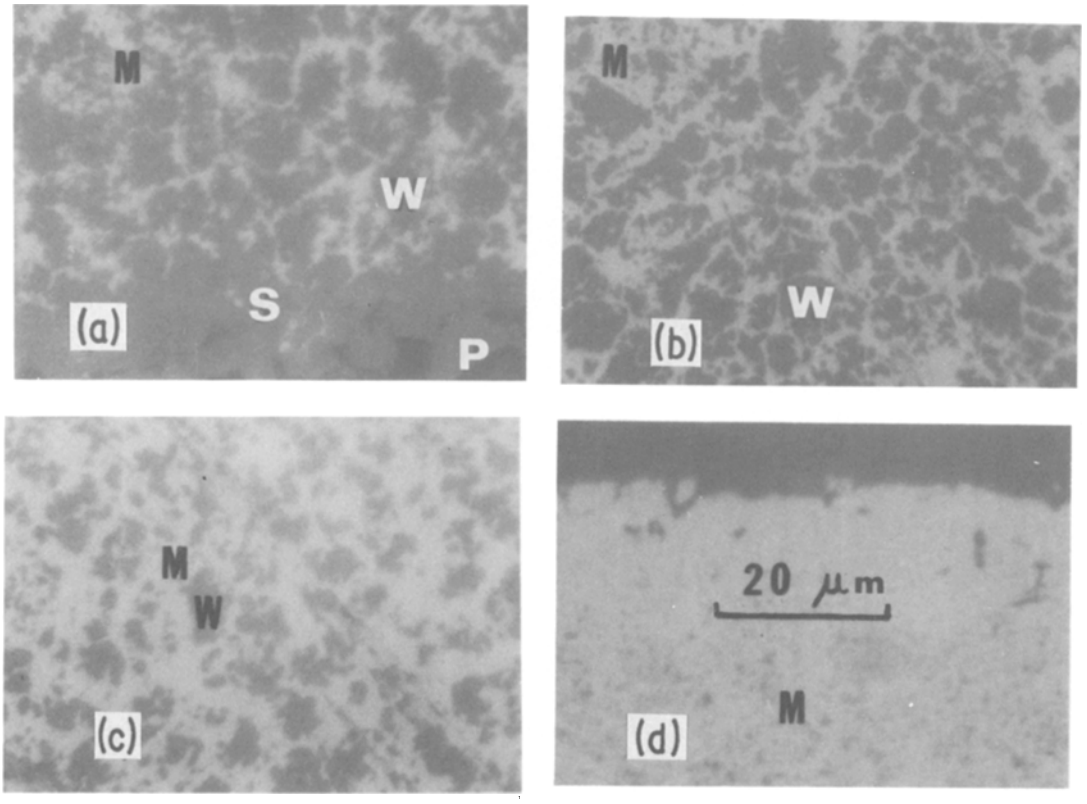

Figure 8 Sequence of optical micrographs of scale cross-section for $NiFe_2O_4$ reacted with hydrogen at 700° C for 5000 sec. (a) interface, (b) near interface, (c) near surface, (d) surface. P: pore (due to pull-out on polishing), S: unreduced spinel, M: porous metal alloy, W: (Ni, Fe)O. The total scale thickness of about 3 mm.

showed that wüstite constituted a small fraction of the retained oxide. At 700° C, this two-phase scale was clearly established and all the retained oxide was identified as wüstite except for a few isolated regions of a partially-reduced nickel-deficient spinel directly at the unreduced oxide–reduced scale interface. A cross section of the product is shown in Fig. 8. It is expected that the phase diagram at this temperature and above is similar to the one shown in Fig. 1 for 1000° C. If wüstite is formed, the scale must be two-phase for such a phase relationship. This is in contrast to $CoFe_2O_4$, where the phase diagram suggests the formation of a distinct single-phase (Co, Fe)O sub-scale. At 800° C the two-phase region of the scale is even more pronounced, as one would expect on the basis of the phase diagram.

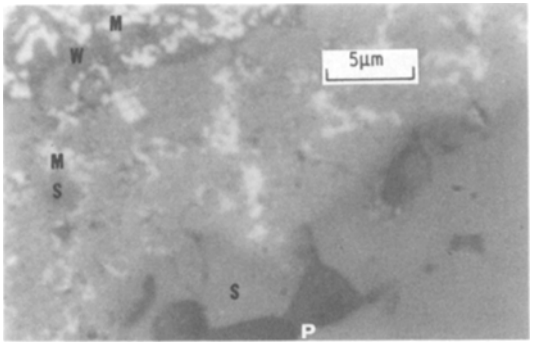

Figure 9 Optical micrograph of etched interface region of $NiFe_2O_4$ after reduction for 1500 sec at 800° C by hydrogen. Two two-phase reaction layers can be observed: M + W and M + S. M: porous metal alloy, S: spinel, W: (Ni, Fe)O, P: pore or pull-out.

A micrograph of an etched interface region after reduction for 1500 sec at 800° C is shown in Fig. 9. Two two-phase reaction layers can be observed: metal plus spinel and metal plus wüstite. The sequence of phases at 800° C is therefore: unreduced spinel–spinel plus metal–wüstite plus metal–metal. At 800° C the phase relationship in the reaction layer corresponds to a vertical section through the $\ln p_{O_2}$-composition diagram, with the NiO-rich phase absent.

Clearly, above 600° C a single-phase, topochemical scale structure is no longer present, and

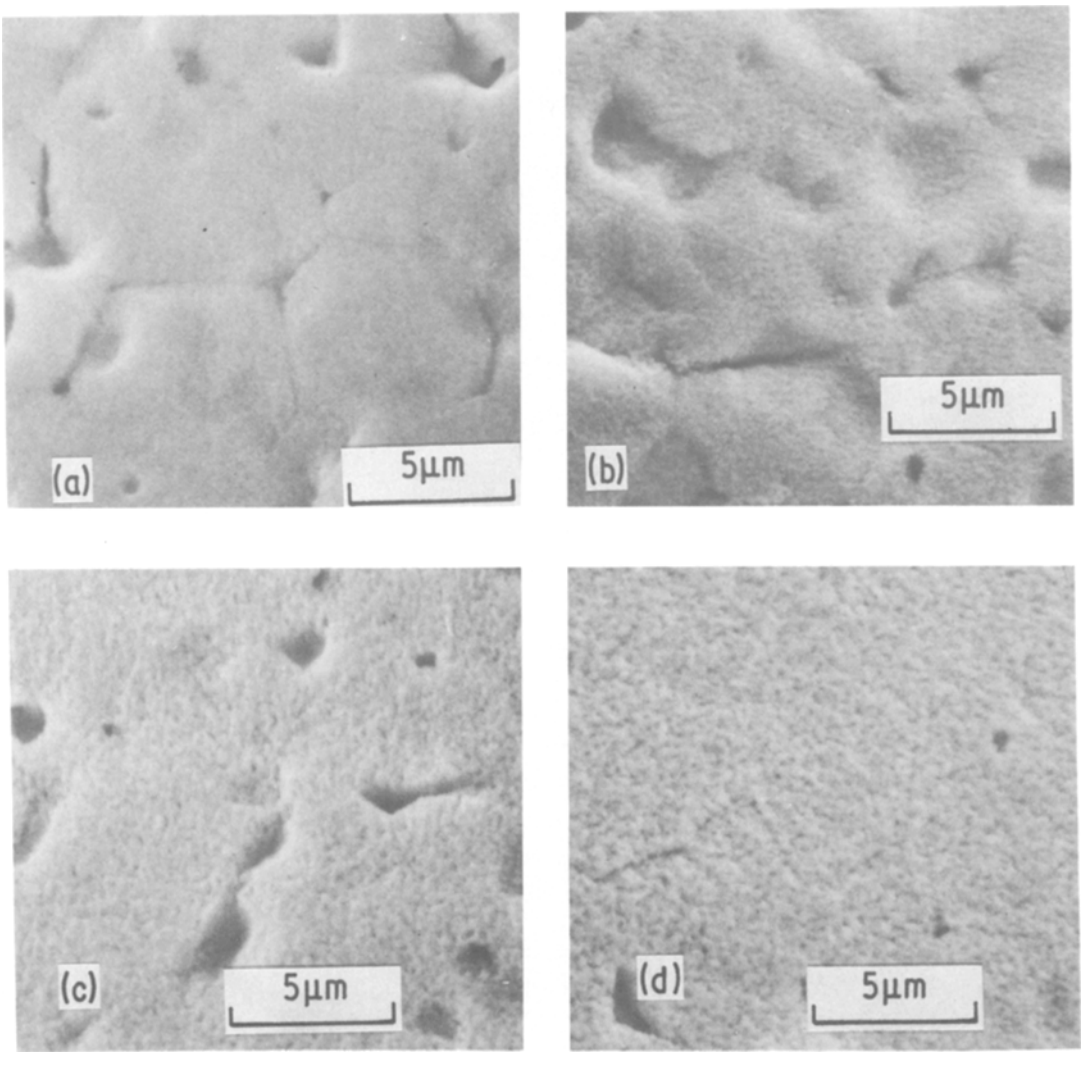

Figure 10 Scanning electron micrographs of surfaces of porous metal product layers on $NiFe_2O_4$ reduced at (a) 450° C, (b) 500° C, (c) 550° C, (d) 600° C. At the lower temperatures the porous metal forms a relic of the original spinel grains.

the two-phase nature of the scale precludes the use of Equation 1 to describe the reduction kinetics.

The evolution of the scale pore structure is shown in Fig. 10 for scales formed between 450° C and 600° C. At the lower temperature the pore structure is bimodal. The scale forms a very finely porous metallic relic of the original spinel grains, with coarse inter-relic pores, as shown in Fig. 11. With increasing reduction temperature, the pores coarsen and the scale evolves to a more uniform structure. This pore structure evolution with increasing temperature causes the behaviour of D_{eff} previously discussed.

3.2.2. $NiAl_{0.02}Fe_{1.9}O_4$

The microstructural aspects of the scales formed on this material are comparable to those of $NiFe_2O_4$. Up to 600° C, a single porous metal product layer is formed. Above 600° C the microstructural sequence is again unreduced: spinel–spinel plus metal–wüstite plus metal–metal. There are some differences, however, from the $NiFe_2O_4$ behaviour: even after reduction for 7000 sec at 600° C the structure is still spinel–metal. At 700° C the presence of Al^{3+} appears to have promoted preferential grain-boundary attack after an initially well-defined interface was formed (Fig.

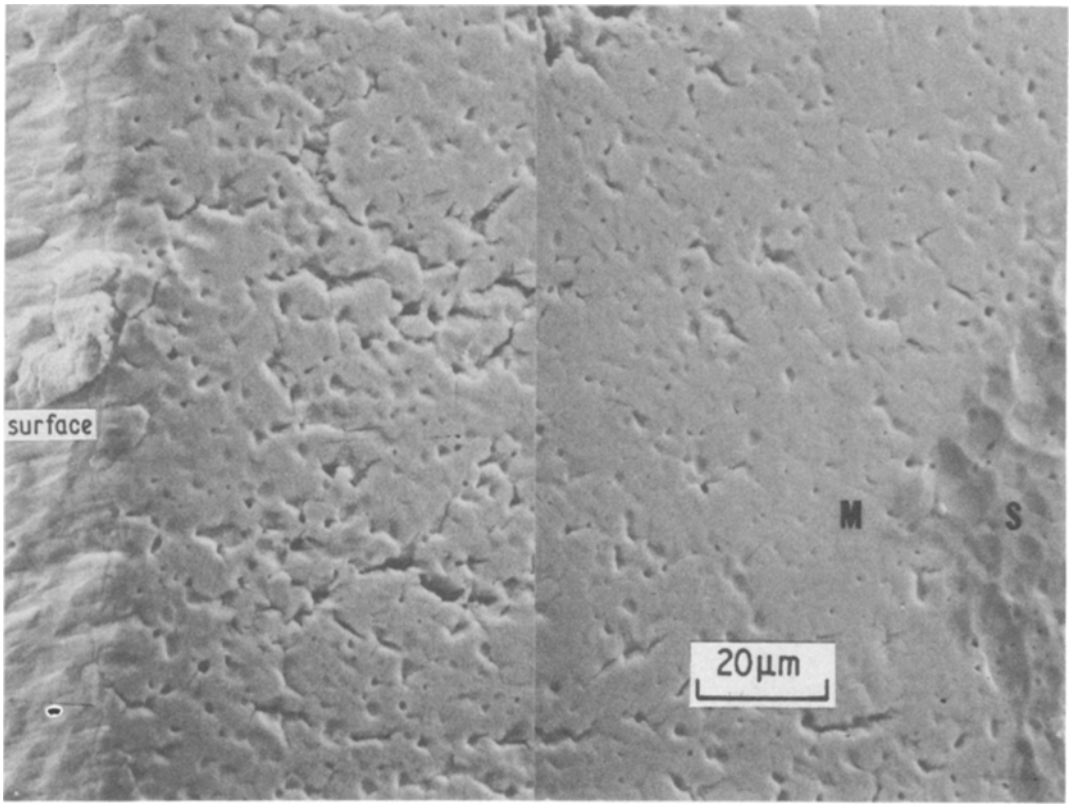

Figure 11 Scanning electron micrograph of cross-section of metal scale formed on $NiFe_2O_4$ at 450° C. M: porous metal alloy, S: spinel. The pore structure in the scale is bimodal: coarse inter-relic pores and very fine relic pores. The surface of the scale is marked and the interface is located between M and S.

12). We believe that this behaviour can be understood by considering the relative rates of the reaction interface advance and of the interface solid-state transport processes. When a ceramic alloy oxide is reduced, the less reducible ion will accumulate ahead of the advancing reaction interface. Since this is a chemical effect that opposes the reaction we can call it "chemical polarization" in analogy with similar electrical phenomena. The degree of accumulation, and thus the interface composition, depends on solid-state transport rates. Similar phenomena are found at the metal–scale interfaces in the oxidation of metal alloys (see, for example, [10]). In the case of oxide reduction by a gas, the product scale–oxide interface velocity depends on the gas composition as well as on the interface composition. To a first approximation, the interface segregation phenomena and the interface velocity can be considered as independent; when the ratio $\dot{\xi}/J_s$ of interface velocity to solid-state diffusion rate, J_s is comparatively high, chemical polarization should develop quickly; when $\dot{\xi}/J_s$ is comparatively low the chemical polarization would be less. Chemical polarization, i.e., the build-up of Fe^{2+} in front of the advancing reaction interface, will slow the interface reaction rate. Preferential grain-boundary reaction will then depend on the ratio of the grain boundary diffusivity to the grain bulk diffusivity, D_{GB}/D_B, as well as on $\dot{\xi}/D_{GB}$. If the ratios $\dot{\xi}/D_{GB}$ and $\dot{\xi}/D_B$ are both comparatively high, chemical polarization rapidly occurs everywhere and a simple interface should be observed. The condition for preferred grain-boundary attack is then that $\dot{\xi}/D_{GB}$ be low and the ratio D_{GB}/D_B be high. We can therefore expect alloy oxides to have a limited range of reaction conditions where grain-boundary attack is pronounced. The location of this régime depends on kinetic parameters that are usually not known *a priori*.

3.2.3. $NiAl_{0.1}Fe_{1.9}O_4$

In this material, a simple spinel–metal structure was observed for all the reaction conditions studied. As in the case of the reduction of $CoAl_{0.1}Fe_{1.9}O_4$ [3], the aluminium led to the formation of un-

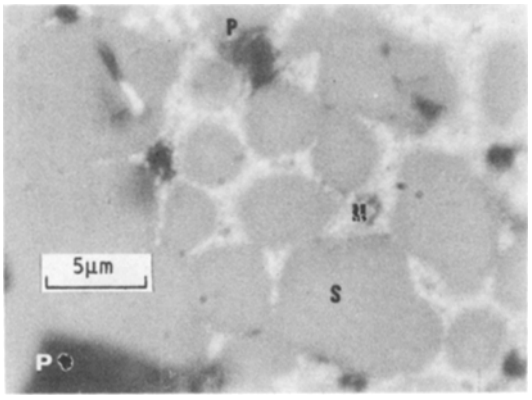

Figure 12 Preferential intergranular reduction in $NiAl_{0.02}Fe_{1.98}O_4$ after reduction for 7000 sec at 600° C. M: porous metal alloy, S: spinel.

reduced oxide particles, dispersed through the metal alloy, that strongly inhibited pore coarsening. The strong grain-boundary attack that was observed for the Al^{3+}-alloyed cobalt ferrites was, however, not found for the alloyed nickel ferrites. This difference in behaviour can be described as in Section 3.2.2.: the ratio $\dot{\xi}/D_{GB}$ is relatively high under these test conditions, while the ratio D_{GB}/D_B is relatively low. As previously reported, significant grain-boundary attack was indeed observed in the reduction of $NiAl_{0.1}Fe_{1.9}O_4$ in flowing Ar–5 vol % H_2 atmosphere at a temperature of 1000° C [11].

4. Conclusions

(a) A simple analysis was presented permitting assessment of the interface reaction resistance and the gas transport resistance through the scale for a topochemical reduction reaction.

(b) $Ni(Al, Fe)_2O_4$ ceramic alloy oxides exhibited mixed reduction reaction control between 450° C and 800° C under a hydrogen pressure of 1 atm. The gas transport resistance in the porous product layer increased in relative importance with increasing temperatures, in the measurement interval.

(c) In a range of temperature and reaction times, preferred grain-boundary reduction was observed. The conditions under which this grain-boundary attack appeared depended strongly on the Al^{3+} content of the $Ni(Al, Fe)_2O_4$. This dependence could be attributed to chemical polarization ahead of the advancing reaction interface. The extent of the chemical polarization depends on the relative magnitudes of the reaction interface velocity and the solid-state diffusion rates.

(d) The phase relationships led to the formation of a two-phase scale when (Fe, Ni)O was present.

(e) As in the reduction of $Co(Al, Fe)O_4$, the presence of Al^{3+} lowered the interface reaction rate and inhibited the scale coarsening.

5. Acknowledgments

Dr D. P. Whittle is thanked for many stimulating discussions. Dr M. Chang assisted in the microstructural observations. A significant part of this work was carried out at Cornell University under DOE Contract EY-76-5-02-2584. Part of this work was also supported by the Basic Sciences Division of the US Department of Energy under Contract W-7405-Eng-48.

References

1. R. H. SPITZER, F. S. MANNING and W. O. PHILBROOK, *Trans. Met. Soc. AIME* **236** (1966) 726.
2. J. R. PORTER and L. C. De JONGHE, *Met. Trans. B*, to be published.
3. U. R. EVANS, *Trans. Electrochem. Soc.* **46** (1924) 247.
4. M. C. REY and L. C. De JONGHE, *J. Mater. Sci.* **15** (1980) 2241.
5. Manlabs Inc., Cambridge, Massachusetts, USA.
6. R. DIECKMANN, T. O. MASON, J. D. HODGE and H. SCHMALZRIED, *Ber. Bunsenger. Phys. Chem.* **82** (1978) 778.
7. J. STICHTER and H. SCHMALZRIED, Report of the Institute of Theoretical Huttenkunde, Technical University of Claustahl, May, 1975.
8. W. -K. LU and G. BITSIANES, *Trans. Met. Soc. AIME* **236** (1966) 531.
9. M. CHANG and L. C. De JONGHE, "Materials Science Research" Vol. 14, edited by J. Pask and A. G. Evans (Plenum Press, New York, 1981).
10. C. WAGNER, *Corrosion Sci.* **9** (1969) 91.
11. J. ALLENDER and L. C. De JONGHE, in "Ceramic Microstructures '76" edited by R. M. Fulrath and J. A. Pask (Westview Press, Boulder, Colarado, 1977) p. 556.

Received 24 October 1980 and accepted 26 March 1981.